Available online at www.sciencedirect.com
SCIENCE DIRECT®
Journal of Crystal Growth 247 (2003) 408–418
JOURNAL OF CRYSTAL GROWTH
www.elsevier.com/locate/jcrysgro

Epitaxial $LiNb_{0.5}Ta_{0.5}O_3$ films on $LiTaO_3$ and $LiNbO_3$ substrates grown by thermal plasma

S.A. Kulinich[a,b,*], T. Yamaki[b,c], S. Bysakh[a], H. Yamamoto[c], K. Mitsuishi[a], M. Song[a], K. Terashima[b,c], K. Furuya[a]

[a] *Nanomaterials Laboratory, National Institute for Materials Science, 3-13 Sakura, 305-0003 Tsukuba, Japan*
[b] *Department of Materials Engineering, Faculty of Engineering, The University of Tokyo, 7-3-1 Hongo, Bunkyo-ku, 113-8656 Tokyo, Japan*
[c] *Department of Advanced Materials Science, Graduate School of Frontier Science, The University of Tokyo, 7-3-1 Hongo, Bunkyo-ku, 113-8656 Tokyo, Japan*

Received 2 August 2002; accepted 3 October 2002
Communicated by M. Kawasaki

Abstract

Single crystal thin films of $LiNb_{0.5}Ta_{0.5}O_3$ were prepared on (0 0 1)$LiTaO_3$ and (0 0 1) $LiNbO_3$ substrates by a thermal plasma spray CVD process using metalorganic precursors. The composition and epitaxial quality of the films, deposited at the growth rate of 20–400 nm/min, were evaluated by transmission electron microscopy and X-ray diffractometry. The surface morphology of the films was characterized by atomic force microscopy in relation to the deposition temperature and the substrate surface conditions.

PACS: 81.15.Gh; 68.55.−a; 61.16.B; 61.10.−i

Keywords: A1. Atomic force microscopy; A1. Transmission electron microscopy; A3. Thin films; B1. Lithium niobate-tantalate

1. Introduction

Lithium niobate ($LiNbO_3$, LN) and lithium tantalate ($LiTaO_3$, LT) are key materials for integrated optics. Their unique nonlinear optical, piezoelectric, pyroelectric, electro-optic and photo-elastic properties make them highly desirable materials in a variety of device applications such as optical modulators and waveguides, surface acoustic wave devices, second-harmonic generators and holographic memory [1–3]. As their solid solution, lithium niobate-tantalate ($LiNb_{1-x}Ta_xO_3$, LNT) possesses intermediate properties (including refractive indices or electro-optic properties) that can be changed by controlling the $x = Ta/(Nb + Ta)$ ratio from those of LN ($x = 0$) to those of LT ($x = 1$). Thus, the key properties of LNT as a material can be adjusted to meet engineering specifications, which makes it a very attractive material for many practical applications [4–8].

*Corresponding author. Tel./fax: +81-3-5841-7103.
E-mail address: kulinich@terra.mm.t.u-tokyo.ac.jp (S.A. Kulinich).

0022-0248/03/$ - see front matter
PII: S0022-0248(02)02013-4

Bulk single crystals of LN and LT are already commonly used in acoustic and optical devices. However, the growth of LNT bulk crystals with high compositional homogeneity and crystallinity by the conventional Czochralski method is difficult because of the wide separation between liquidus and solidus lines in the LN–LT phase diagram. Therefore, high-quality LNT films fabricated with good compositional control on appropriate substrates are highly desirable.

During the past decade, as interest in thin ferroelectric film devices has grown dramatically, the fabrication of both non-doped [2,7–16] and doped [10,17–19] LN and LT films on various substrates has been intensively investigated for the preparation of highly integrated optical and electro-optic devices. A number of deposition techniques have been explored, including metalorganic CVD (MO CVD) [2,13–15], liquid-phase epitaxy (LPE) [7–10,20,21], pulsed laser deposition (PLD) [11,12], sol–gel processing [4,16,19,22] and so forth. At the same time, there have been only a few reports on LNT film fabrication. Kawaguchi et al. reported LNT film growth on LN substrates with $0<x<0.4$, using the LPE method [7–9]. In their experiment, film crystallinity degraded significantly at $x>0.3$, corresponding to an increase of lattice mismatch and growth temperature [7]. More recently, Cheng et al. grew highly (0 0 6)-oriented LNT films with $x<0.33$ on Si(1 1 1) substrates, using the sol–gel technique [4], and also found that the degree of orientation was relatively low when $0.5\leqslant x<1$.

$LiTaO_3$ and $LiNbO_3$, as substrate materials for LNT films, have two important advantages over the more common sapphire: both their lattice constants (mismatch of 0.1–0.3% along the *a*-axis, depending on film *x*) and thermal expansion coefficients are much closer to those of LNT material. Therefore, much higher LNT film quality is expected on such highly lattice-matched substrates.

A thermal plasma spray CVD (TPS CVD) method, which has been developed for various multi-component film fabrications, has several advantages [23] including: a large number of potential materials and dopants, continuous and accurate control of feeding rate of the liquid source materials into the plasma, large-area film deposition, comparatively high growth rate (tens to hundreds of nm/min), easy compositional control by using liquid source materials, and compositional homogeneity among others. We have recently reported the deposition of epitaxial LNT films on sapphire [24,25] and highly oriented LNT films on Si [26,27] substrates by the TPS CVD process using a liquid metalorganic solution.

The aim of this work was to study the TPS CVD process for LNT films on highly lattice-matched (0 0 1)LT and (0 0 1)LN substrates, in order to develop this technique for the fabrication of crystalline films with device qualities in the future. Although single-crystal LN and LT [2,10,13, 14,20–22] and LNT ($0\leqslant x\leqslant 0.3$) [7–9] thin films have been previously prepared on LT or LN substrates, including 5 mol% MgO-doped LN [10,22], using mainly MO CVD [2,13,14], sol–gel [22] and LPE [7–10,20,21] techniques, we present herein the first report on LNT films prepared at comparable or even higher growth rates and higher Ta content $x=0.5$.

2. Experimental details

As-supplied single-crystal (0 0 1)LT (MolTech GmbH, Germany) and (0 0 1)LN (Earth Chemical Co., Ltd., Japan) optically polished plates $10\times 10\times 0.5\,mm^3$ in size were used as substrates. Prior to film growth, the substrates were ultrasonically cleaned and rinsed with acetone and ethanol. Additionally, a number of LT and LN wafers heat-treated in air at 800°C, 900°C and 1000°C for 1 h were used as substrates for comparison. The liquid precursor used was a uniform mixture of metalorganic alkoxides, $LiTa(OR)_6$ and $LiNb(OR)_6$ in 3-methylbutyl acetate solvent, which were obtained from Kojundo Chem. Lab. Co., Japan. The concentration of metals in each individual precursor solution corresponded to 3 wt% $LiTaO_3$ or $LiNbO_3$, respectively. As reported in our earlier works, a mixture of these solutions with the initial ratio Ta:Nb = 1:1 yielded single-phase $LiNb_{1-x}Ta_xO_3$ films with $x=0.5$ on sapphire and silicon substrates [24–27]. Therefore, this source composition

was also used in this work. The TPS CVD process using O_2–Ar radio frequency thermal plasma was applied for film preparation. The details of film fabrication, plasma chamber description, as well as the method itself, have been given elsewhere [23,24,26]. The main growth parameters are summarized in Table 1.

The microstructure and interface between the film and the substrate were studied by transmission electron microscopy (TEM), and energy-dispersive X-ray spectroscopy (EDS) with a probe of 1 nm size was applied to evaluate the chemical composition of the films. The cross-sectional samples for electron microscopy were prepared by conventional procedures including specimen gluing, cutting and polishing, followed by ion milling, as reported elsewhere [22,25]. The specimens were investigated using a JEOL JEM-2010F electron microscope with a field emission gun operated at 200 kV and a JEOL ARM-1000 high-voltage electron microscope operated at 1000 kV. Film thickness was estimated by cross-sectional scanning electron microscopy (SEM). The samples for SEM examination were prepared by coating with 2 nm of Au or carbon and were then placed in a Hitachi S-4200 field emission SEM and examined at an accelerated voltage of 10 kV.

In order to evaluate the morphological surface features of the films and the substrates, atomic force microscopy (AFM) analysis was performed in the tapping mode with a Si tip using a Digital Instruments NanoScope IIIa system. Because the LT and LN substrates might be pyroelectrically charged, to prevent such a charging during AFM observation, the samples were fixed to the steel stage using a silver paste with their surface hemmed in by the silver paste, leaving a window for observation that was approximately $1 \times 1\,mm^2$ in size, following the work of Nagata et al. [28]. In order to examine the LNT film phase composition and epitaxial orientation, X-ray diffraction (XRD), conventional $2\theta/\theta$ scanning and $2\theta\chi/\varphi$ scanning at a small incidence angle of 0.35°, was performed.

Table 1
Summary of experimental conditions

Source Li:Nb:Ta ratio	2:1:1
Plasma pressure (Torr)	150
Plasma power (kW)	46.2
O_2 tangential gas flow rate (l/min)	45.0
Ar inner gas flow rate (l/min)	5.0
Ar carrier gas flow rate (l/min)	3.0
Ar spray gas flow rate (l/min)	3.6
Torch–substrate distance (cm)	37
Substrate temperature, T_{sub} (°C)	590–720
Liquid precursor feed rate (ml/min)	0.5–8.0
Film growth rate (nm/min)	20–400
Deposition time (min)	0.5–8.0
Typical film thickness (nm)	100–200
Substrate	(0 0 1)LT, (0 0 1)LN

3. Results and discussion

3.1. Film–substrate interface

In order to investigate the distribution of Ta and Nb through out the film–substrate interface and the depth of the sample, EDS microprobe measurements were carried out. Figs. 1a and b are

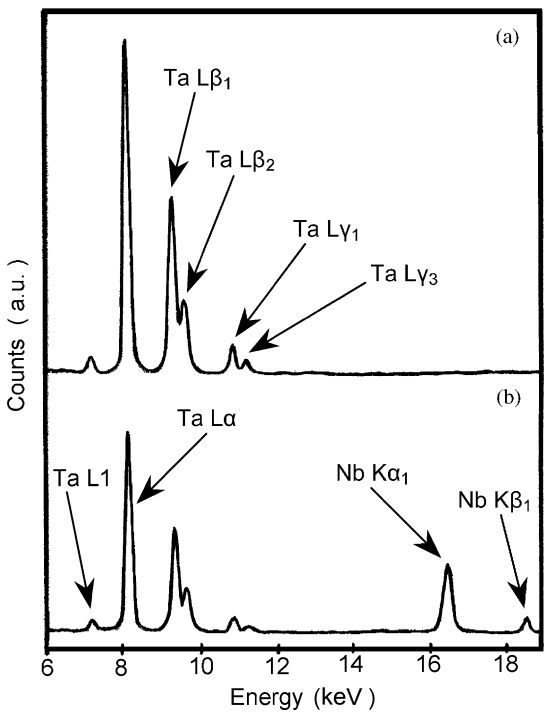

Fig. 1. EDS spectra of the 100-nm-thick LNT film on as-received LT grown at 100 nm/min and $T_{sub} = 595 \pm 5$°C: (a) LT substrate area, (b) LNT film area.

examples of typical EDS spectra for the LT substrate (a) and the LNT film (b) areas for a sample fabricated at 100 nm/min and $T_{sub} = 595 \pm 10^{\circ}C$ for 1 min on as-supplied LT substrate. The composition distributions of Ta and Nb atoms were found to be uniform within both the film and the substrate, and no Nb was detected within the LT substrate (Fig. 1a). Thus, a good step profile at the LNT//LT interface can enable a sharp-stepped refractive index profile for the sample.

Cross-sectional high-resolution TEM (HRTEM) of the same specimen reveals good epitaxial growth behavior, as seen in Fig. 2a. In contrast to (0 0 1)LN films on (0 0 1) sapphire, where misfit dislocations were normally found by TEM at the interface [11,22], the HRTEM micrograph in Fig. 2a demonstrates no evidence of the formation of misfit dislocations. The interface between the LNT film and LT substrate seems to be coherent. This was expected, because good matching of the film and the substrate in terms of the lattice parameters and the thermal expansion produces stresses at the interface, which may be too weak to introduce a large number of misfit dislocations, compared to the case of LN on sapphire.

The selected area electron diffraction (SAED) pattern (Fig. 2b) corresponding to the LNT//LT interface of the same sample also confirms the epitaxial growth and demonstrates no weak extra spots caused by twin structures or any additional phases within the interface area of the sample.

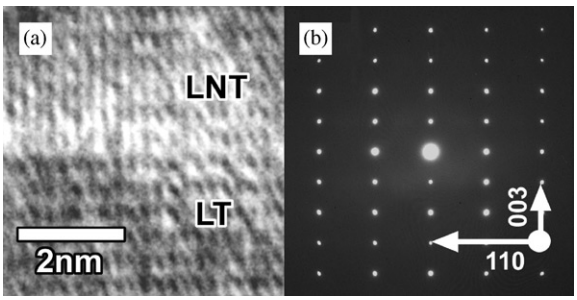

Fig. 2. (a) Cross-sectional HRTEM image of the 100-nm-thick LNT film on as-received LT grown at 100 nm/min and $T_{sub} = 595 \pm 5^{\circ}C$. (b) SAED pattern of the LNT//LT interface for the same sample. The zone axis is [$\bar{1}$ 1 0].

Owing to a very small lattice parameter mismatch between LT and LNT materials, no shifts of reflection positions between the LNT film and the LT substrate are observed in Fig. 2b.

Our TEM observations are in good agreement with those of Terabe et al. [22] who analyzed sol–gel-grown LN films on various substrates, including LT, suggesting the decrease in the number of structural defects in LNT ($0 \leqslant x \leqslant 1$) films on highly lattice-matched substrates regardless of the growth techniques employed.

3.2. Phase composition and in-plane alignment

The growth rates, as evaluated from the cross-sectional SEM analyses of the film thickness, were deduced to linearly vary within the range of 20–400 nm/min, when the liquid feed rate applied was increased from 0.5 to 8 ml/min, which is in good agreement with those for the previously reported TPS-CVD-fabricated LNT films on sapphire [24] and silicon [26,27] substrates.

Unlike LNT films grown by TPS CVD on sapphire, where the (0 0 1) orientation of films was notably governed by the growth temperature and rate and was improved when the latter was held at 180–400 nm/min [24], our present results demonstrate no significant influence of growth rate on film orientation at substrate temperatures within the applied range of $590 < T_{sub} < 720^{\circ}C$. This is believed to be caused by the difference in the lattice mismatch between the two systems, i.e., (0 0 1)LNT//(0 0 1)α-Al_2O_3 (mismatch on the order of 8% [11]) and (0 0 1)LNT//(0 0 1)LT or (0 0 1)LN (mismatch on the order of 0.1–0.3% [14]).

Fig. 3a shows the XRD pattern of the LNT film grown at 50 nm/min and $T_{sub} = 625 \pm 5^{\circ}C$. The X-ray diffraction of this LNT//LN sample reveals the presence of highly (0 0 1)-aligned epitaxial LNT on the single crystal (0 0 1)LN wafer. No polycrystalline or other phases are detected by the XRD $2\theta/\theta$ scan. However, since the fabricated films were normally 180–200 nm thick, it was impossible to discriminate their peaks from those of the substrate by means of the conventional XRD film technique, as seen in Fig. 3a. Fig. 3b

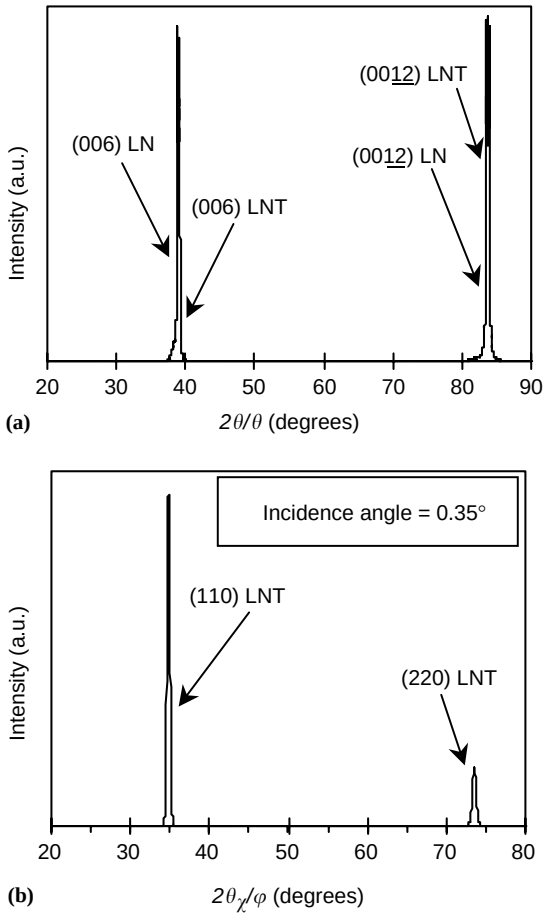

Fig. 3. XRD $2\theta/\theta$ scan pattern (a) and in-plane $2\theta\chi/\varphi$ scan pattern (b) of the 190-nm-thick $LiNb_{0.5}Ta_{0.5}O_3$ film on as-received LN substrate, deposited at 50 nm/min and $T_{sub} = 625 \pm 5$°C. The incidence angle used for (b) was 0.35°.

presents the spectrum obtained by XRD $2\theta\chi/\varphi$ scanning of the same specimen, performed at a small incidence angle of 0.35°, which may also evaluate the film's in-plane orientation. It is seen that only vertical film (1 1 0) and (2 2 0) crystallographic planes are detected. This provides further evidence that the LNT film has a single-crystal structure and is in-plane aligned with the LN substrate with no detectable twinning, which is quite common for LNT ($0 \leqslant x \leqslant 1$) films fabricated on a (0 0 1) sapphire substrate with much larger lattice mismatch and difference in thermal expansion coefficients [2,11,15,22,24,29].

3.3. Surface morphology

Thin-film surface morphology and roughness are important for many applications, and especially for waveguides. As previously reported [3,15], optical and electrical properties of ferroelectric films are strongly affected by their structural defects and surface morphology. To achieve comparable performance with bulk single-crystal waveguide devices, high-quality LNT films should be grown single-crystalline and with low surface roughness. Previous work has shown that surface scattering can account for up to 50% of the optical loss in a thin film [3]. Therefore, to compete with bulk single-crystal waveguide devices, the film root-mean-square roughness (R_{rms}) should be on the order of 1.0 nm, such that the optical losses are lower than 1.0 dB/cm [3,15]. Thus, understanding the development of morphological features and roughness tendencies in thin-film structures is very important for controlling optical losses.

The effect of substrate temperature (T_{sub}) on surface roughness of LNT films on as-received (0 0 1)LN substrates is given in Fig. 4, as measured by AFM for surface areas of $2 \times 2\,\mu m^2$. Since, in general, surface roughness is significantly affected by film thickness and other deposition parameters, all the samples were grown at the same growth rate of 180–200 nm/min and had similar thicknesses of approximately 180–200 nm. As the average deposition temperature increases from 595°C to about 680°C, the surface R_{rms} of the films decreases. However, at $T_{sub} > 680$°C, the film surface starts to roughen again. Although the reason for this is not yet clear, the similarity to the MO-CVD-prepared LN films on (0 0 1) sapphire reported by Lee and Feigelson [15] is obvious. Moreover, a similar trend for film surface flattening with increasing substrate temperature within the range of $510 \leqslant T_{sub} \leqslant 675$°C was also reported by Feigelson [2] for LN films on (0 0 1)LT wafers. The above temperature-dependent surface improvement was suggested to be related to the increase in the surface mobility of the deposited species at elevated substrate temperatures [2]. However, the surface roughness of LN films deposited on LT at $T_{sub} > 675$°C was not measured [2], and probably

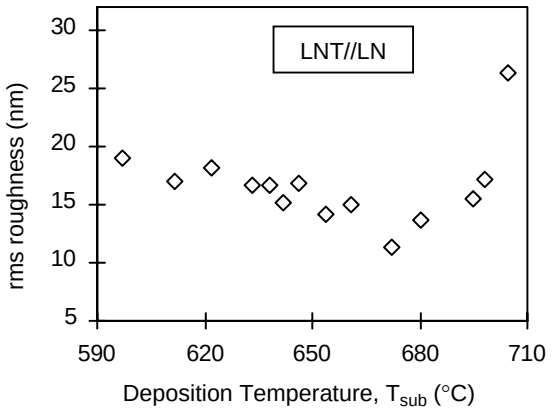

Fig. 4. Film root-mean-square roughness as a function of average deposition temperature for 180–200-nm-thick LNT films deposited at 180–200 nm/min on as-received (0 0 1)LN wafers.

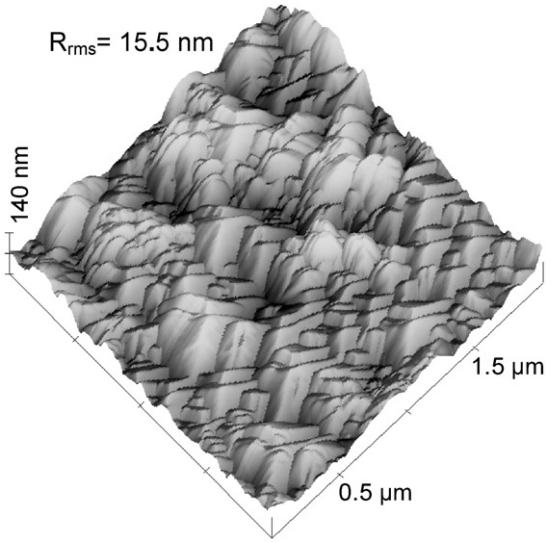

Fig. 5. AFM surface image ($2 \times 2\,\mu m^2$) of LNT film on as-received LN substrate grown at 50 nm/min and $T_{sub} = 695 \pm 5^{\circ}C$ for 4 min. Three-fold symmetry of the surface-forming islands is revealed.

this could be a reason that further film roughening was not detected.

Fig. 5 presents typical surface morphology for the 190-nm-thick LNT film on as-supplied LN grown at a relatively high deposition temperature of $T_{sub} = 695 \pm 5^{\circ}C$ and at a growth rate of 50 nm/min. The surface area of $2 \times 2\,\mu m^2$ is shown. While surface roughness is somewhat increased compared to those for the films fabricated at $T_{sub} < 680^{\circ}C$, it is seen that the surface consists of in-plane-aligned triangular pyramids whose three-fold symmetry is typical for LNT single crystal (trigonal symmetry group). The pyramidal faces are believed to be the {0 1 2}LNT planes, by analogy with the (0 0 1)LN islands observed at the early stages of growth on (0 0 1) sapphire by Veignant et al. [11].

Another key factor contributing to film smoothness may be the surface and quality of the substrate used. It is known that as-supplied LT and LN substrates, which are produced by the mechanochemical mirror polishing process, have irregular corrugations and crystallographic defects on their topmost surface [28]. Consequently, the atomic-scale flatness of the substrate surface caused by high-temperature annealing of commercial LT and LN wafers is expected, based on analogy with α-Al_2O_3 [12,30], to enhance the epitaxial growth of the LNT films [28]. As suggested by Yoshimoto et al. [30] and Lee et al. [12], pre-deposition flattening of the sapphire substrate surface might result in sharp interfaces and, thus, better quality of fabricated devices. However, little is known about the quality and the surface-preparation procedures of LT and LN substrates used in the growth of oxide films. Also, no experimental information is available on the relationship between film quality and substrate surface condition [2].

In Figs. 6a and b, the surface topographies of as-received (0 0 1)LT (a) and (0 0 1)LN (b) are given. The two AFM images reveal a number of nano-scratches and corrugations caused by mechanochemical polishing of the optical-grade surface. Fig. 6c shows the AFM surface morphology of a 100-nm-thick LNT film deposited on an as-received LT wafer, where two rows of somewhat higher LNT islands are seen. It is believed that these island rows have formed along the nano-scratches of the substrate surface (see Figs. 6a and b), which probably provided nucleation sites with lower energy. Even though the above LNT islands were not clearly detected on the surfaces of thicker (180–200 nm) films, it is obvious that they still

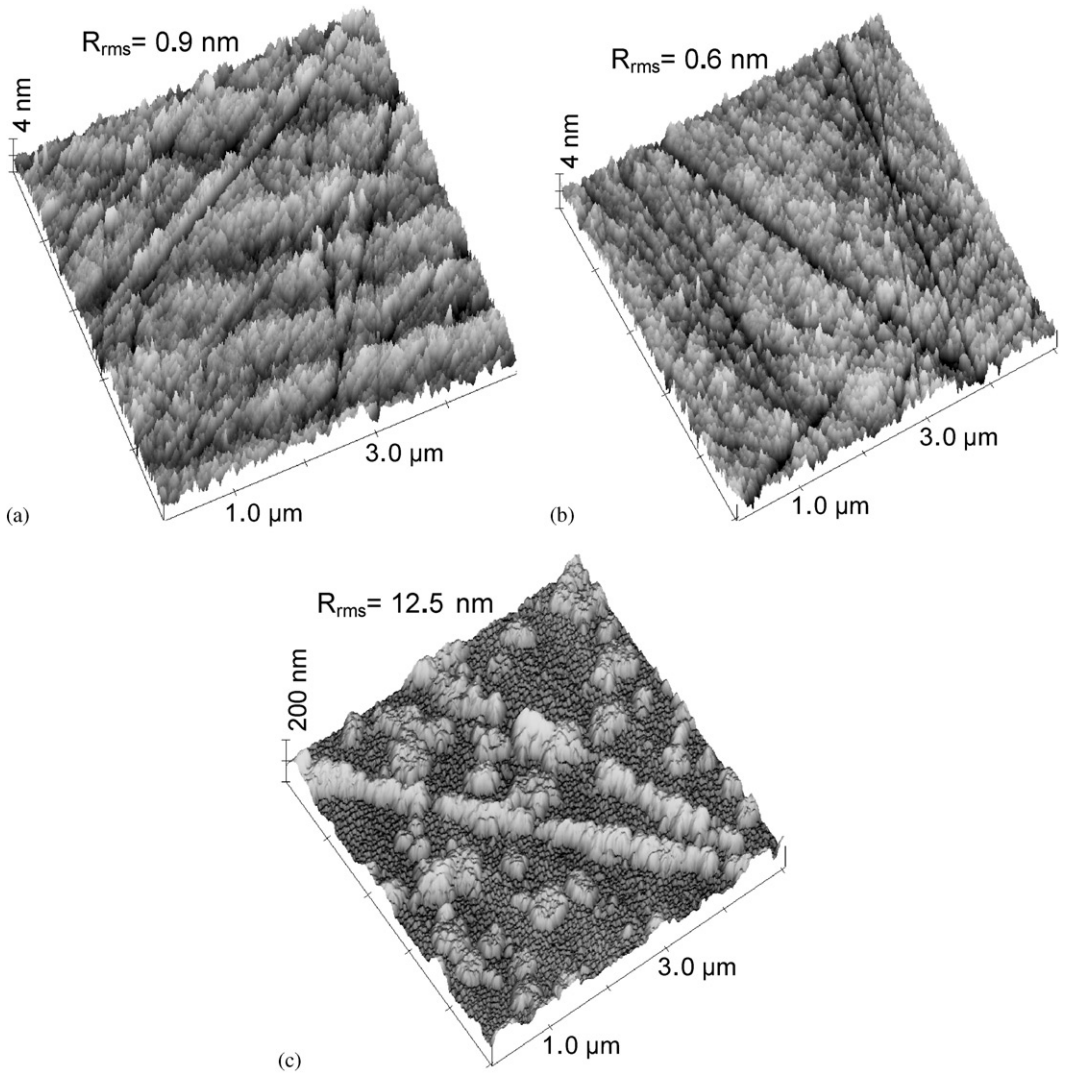

Fig. 6. AFM surface images ($5 \times 5\,\mu m^2$) of the as-received LT (a) and LN (b) substrates. Numerous nano-scratches and corrugations of the surfaces are seen. (c) AFM surface image ($5 \times 5\,\mu m^2$) of the LNT film deposited on as-received LT substrate at 100 nm/min and $T_{sub} = 595 \pm 10^{\circ}C$ for 1 min. Rows of high islands formed along substrate surface scratches are clearly seen.

contributed to the film roughening when as-supplied substrates were used.

Fig. 7 shows the R_{rms} surface roughness (evaluated for $2 \times 2\,\mu m^2$) of LNT films deposited on LN (a) and LT (b) substrates as a function of substrate annealing temperature (T_{anneal}) performed in air for 1 h. All the films, 180–200-nm thick, were grown at $T_{sub} = 650 \pm 10^{\circ}C$ and 180–200 nm/min. The R_{rms} values for the films grown on as-received substrates correspond to $T_{anneal} = 25^{\circ}C$. The roughness dependencies in Fig. 7, which cannot be explained as yet, seem to be related to the nucleation density of the growing films at a very early stage of their formation. It should be noted that even for the quasi-homoepitaxial system LN//LT, as shown by Feigelson [2], a three-dimensional island growth mode is realized in the case of vapor deposition. The number of

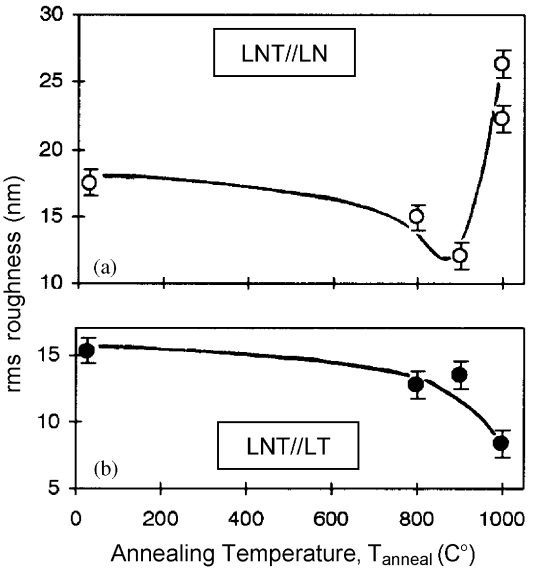

Fig. 7. LNT film root-mean-square roughness as a function of LN (a) and LT (b) substrate pre-deposition annealing temperature in air. All the films, 180–200 nm thick, were grown at $T_{sub} = 650 \pm 10$°C and 180–200 nm/min. Solid lines are added only as visual guides.

nucleation sites on high-temperature-treated LN substrate with well-defined surface steps (reconstructed LN, see Fig. 8a) might be lower than that on as-received LN, as previously reported for the (0 0 1) sapphire substrate [2]. The steps in Fig. 8a provide lower energy sites for film nucleation than the terraces. Thus, under sufficiently high temperature conditions, when the species can reach the steps quite fast, the number of nuclei is expected to be smaller. As a result, the average grain size becomes larger, which, in general, leads to increased surface roughness [15].

On the other hand, some surface flattening of the LNT films on the annealed wafers, as expected, could result from the disappearance of the surface nano-scratches, which is indeed observed in Fig. 7 for the films grown on LN and LT wafers annealed at $T_{anneal} \leqslant 900$°C and $T_{anneal} \leqslant 1000$°C, respectively. Fig. 8 shows the AFM surface topography of both LN (a) and LT (b,c) substrates, measured after annealing in air at 1000°C for 1 h. It is seen in Fig. 8a that the surface restructuring of (0 0 1) LN took place after heat treatment. While surface nano-scratches observed in Fig. 6b disappeared, a set of very regular steps with atomically flat terraces, highly similar to those previously reported for high-temperature-treated (1300–1400°C) (0 0 1) sapphire [2,12,15,30], was formed instead. The terraces are about 200–400 nm wide and 0.23 nm high, which corresponds to $\frac{1}{6}$ of the c-parameter of the LN unit cell ($c = 13.86$ Å) or the minimum distance between two oxygen planes of the layered LN structure [1]. It is believed that, as described above, these terraces could be the reason for the increased LNT film roughness presented in Fig. 7a. At the same time, Figs. 8b and c reveal only the initial formation and growth of well-regulated steps on LT surface, which are very similar to the results of Nagata et al. [28] for high-temperature-treated (900–1000°C) LN wafers. Note that for convenience, two different surface areas, 2×2 and $5 \times 5\,\mu m^2$, for LT are presented in Figs. 8b and c. While Figs. 8a and b allow comparison of the state of LN and LT surfaces after thermal treatment, Fig. 8c, in comparison with Fig. 6a, clearly shows the surface flattening and disappearance of the majority of nano-scratches. It is likely that it is the difference in surface morphology of the annealed LN and LT substrates (Fig. 8) that plays a key role in the difference in LNT film nucleation, growth and roughening on them (Fig. 7). Whereas the surface of the LN substrate is very uniform, some relatively deep scratches on the LT wafer have not yet disappeared after heating at 1000°C for 1 h. The annealing conditions applied (1000°C, 1 h) seemed to be insufficient for LT to reach such a regular surface as in the case of LN, which correlates well with both the difference in melting point and the initial surface conditions of the LN and LT materials. On the other hand, this correlates well with the results in Fig. 7; namely, since most of the nano-scratches on the LT surface have vanished at 1000°C, the roughness of the LNT film on such a wafer is lower, while it started to increase on the LN substrates, where a very regular surface is formed, leading to a lower film nucleation density.

As mentioned above, neither the characteristics of the substrates for oxide-film fabrication nor the surface-preparation procedures have been

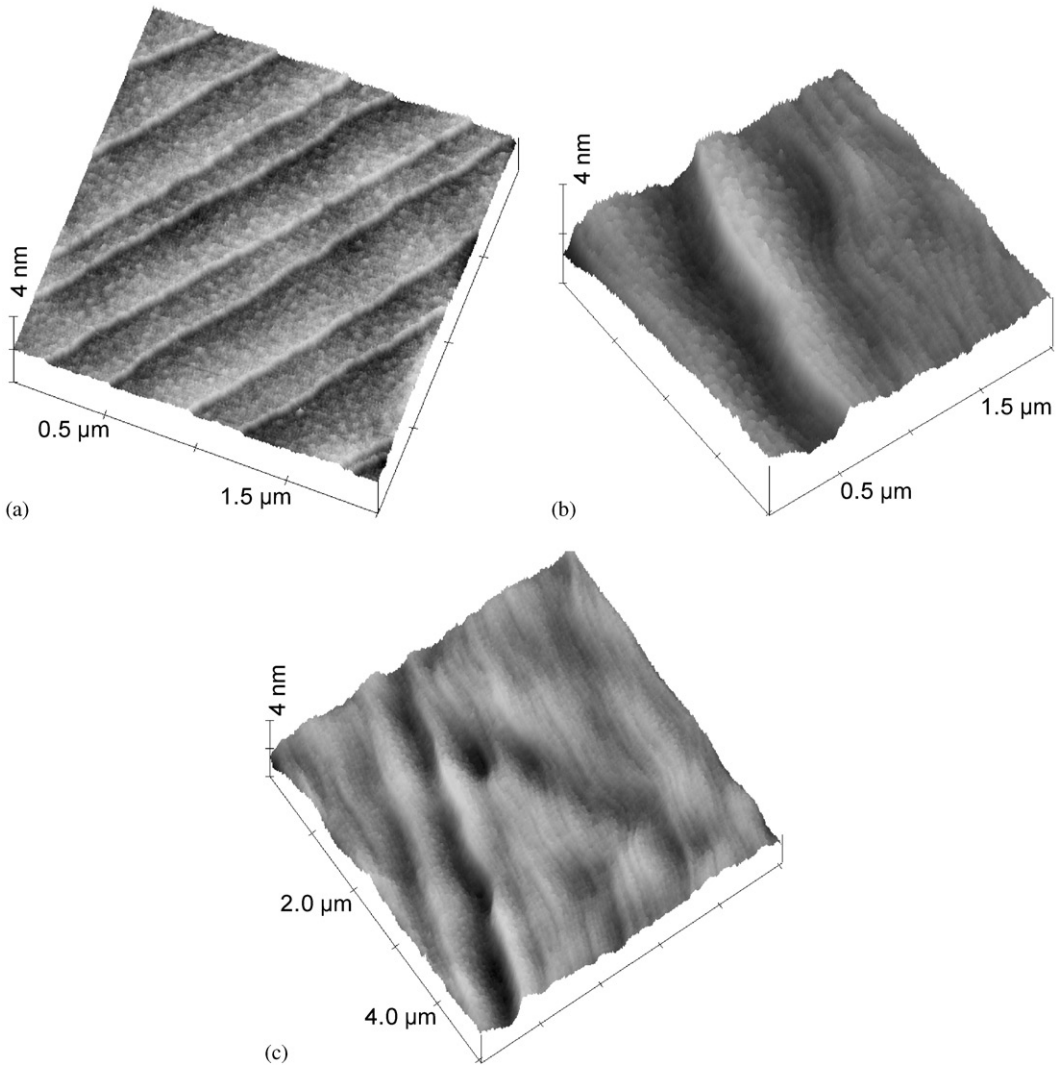

Fig. 8. AFM surface images of the LN (a) and LT (b,c) substrates heat-treated at 1000°C for 1 h in air. Surface areas of $2 \times 2\,\mu m^2$ (a,b) and $5 \times 5\,\mu m^2$ (c) are shown.

carefully investigated thus far with respect to the properties and qualities of the deposited films. While the pre-deposition heat treatment of sapphire substrates was reported by several groups [2,12,15,30], there are only a few works on LN or LT as potential substrates. As an example, Nagata et al. [28] studied the influence of dry atmosphere annealing on the surface morphology of (0 0 1)LN, which consequently can affect the fabricated film epitaxy, microcrystallinity and morphology. They revealed the importance of controlling surface OH content as an additional key factor governing LN surface morphology during and after thermal treatment. Our present results also reveal the importance of substrate surface control and optimization before high-quality films are grown. As was shown above, the substrate surface condition is of great

importance for realizing the designed LNT film surface morphology.

It was unexpected, however, that the roughness of high-rate-grown LNT films on LT and LN wafers was of the same order as those on silicon and sapphire reported previously [24,27], and still remained high for any waveguide devices. This implies that surface roughness evolution for thermal-plasma-grown LNT films is likely to be caused by some reasons other than the nature of the substrate, and further experimental studies are necessary to better understand the mechanisms involved in film roughening and to improve surface smoothness.

4. Summary

Thermal-plasma-grown $LiNb_{0.5}Ta_{0.5}O_3$ epitaxial thin films on (0 0 1)$LiTaO_3$ and (0 0 1)$LiNbO_3$ substrates were characterized by X-ray diffractometry, transmission electron microscopy, energy-dispersive X-ray spectroscopy and atomic force microscopy. Single-phase and single-crystalline films 100–200 nm thick were deposited from oxygen–argon thermal plasma using metalorganic liquid precursors, and their surfaces were crack-free. The surface roughness of the films was found to vary considerably with deposition temperature and substrate surface conditions, thus implying the importance of careful optimization and control of these two parameters. Our results suggest that the thermal plasma spray CVD method can be a promising technique for preparing ferroelectric films, although further investigations are needed to decrease surface roughness of the resulting films.

Acknowledgements

The authors would like to thank Prof. T. Yoshida (The University of Tokyo) for his inspiration and fruitful discussions. The assistance of Y. Shimada (The University of Tokyo), and Y. Nakayama and Dr. Y. Toda (NIMS) is also appreciated. This work was partially supported by the Japan Society for the Promotion of Science (JSPS) under the program "Research for the Future" (JSPS-RFTF # 97R15301).

References

[1] R.S. Weis, T.K. Gaylord, Appl. Phys. A 37 (1985) 191.
[2] R.S. Feigelson, J. Crystal Growth 166 (1996) 1.
[3] D.K. Fork, F. Armani-Leplingard, J.J. Kingston, MRS Bull. 21 (7) (1996) 53.
[4] S.D. Cheng, C.H. Kam, Y. Zhou, X.Q. Han, W.X. Que, Y.L. Lam, Y.C. Chan, J.T. Oh, W.S. Gan, Thin Solid Films 365 (2000) 77.
[5] D. Xue, K. Betzler, H. Hesse, Solid State Commun. 115 (2000) 581.
[6] R.E. Cohen, J. Phys. Chem. Solids 61 (2000) 139.
[7] T. Kawaguchi, H. Kitayama, M. Imaeda, S. Ito, K. Kaigawa, T. Taniuchi, T. Fukuda, J. Crystal Growth 169 (1996) 94.
[8] K. Kaigawa, T. Kawaguchi, M. Imaeda, H. Sakai, T. Fukuda, J. Crystal Growth 191 (1998) 119.
[9] T. Kawaguchi, M. Imaeda, M. Minakata, T. Taniuchi, T. Fukuda, J. Crystal Growth 166 (1996) 489.
[10] A. Yamada, H. Tamada, M. Saitoh, J. Crystal Growth 132 (1993) 48.
[11] F. Veignant, M. Gandais, P. Aubert, G. Garry, J. Crystal Growth 196 (1999) 141.
[12] G.H. Lee, M. Yoshimoto, H. Koinuma, Appl. Surf. Sci. 127–129 (1998) 393.
[13] A.A. Wernberg, G.H. Braunstein, G. Paz-Pujalt, H.J. Gysling, T.N. Blanton, Appl. Phys. Lett. 63 (1993) 331.
[14] A.A. Wernberg, H.J. Gysling, G. Braunstein, J. Crystal Growth 140 (1994) 57.
[15] S.Y. Lee, R.S. Feigelson, J. Crystal Growth 186 (1998) 594.
[16] S. Ono, S. Hirano, J. Mater. Res. 16 (2001) 1155.
[17] J.B. Shim, N. Yoshimoto, D.H. Yoon, J. Crystal Growth 235 (2002) 640.
[18] T. Kawaguchi, K. Mizuuchi, T. Yoshino, M. Imaeda, K. Yamamoto, T. Fukuda, J. Crystal Growth 203 (1999) 173.
[19] S. Ono, T. Takeo, S. Hirano, J. Am. Ceram. Soc. 79 (1996) 1343.
[20] D. Callejo, S. Manotas, M.D. Serrano, V. Bermudez, F. Agullo-Rueda, E. Dieguez, J. Crystal Growth 226 (2001) 488.
[21] V. Bermudez, M.D. Serrano, E. Dieguez, J. Crystal Growth 198/199 (1999) 526.
[22] K. Terabe, A. Gruverman, Y. Matsui, N. Iyi, K. Kitamura, J. Mater. Res. 11 (1996) 3152.
[23] N. Yamaguchi, T. Hattori, K. Terashima, T. Yoshida, Thin Solid Films 316 (1998) 185.
[24] H. Yamamoto, S.A. Kulinich, K. Terashima, Thin Solid Films 390 (2001) 1.
[25] D.V. Shtansky, S.A. Kulinich, K. Terashima, T. Yoshida, Y. Ikuhara, J. Mater. Res. 16 (2001) 2271.

[26] S.A. Kulinich, J. Shibata, H. Yamamoto, Y. Shimada, K. Terashima, T. Yoshida, Appl. Surf. Sci. 182 (2001) 150.
[27] S.A. Kulinich, H. Yamamoto, J. Shibata, K. Terashima, T. Yoshida, Thin Solid Films 407 (2002) 60.
[28] H. Nagata, K. Shima, J. Ichikawa, J. Am. Ceram. Soc. 80 (1997) 1203.
[29] J. Shibata, H. Yamamoto, S.A. Kulinich, T. Yamamoto, K. Terashima, T. Yoshida, Y. Ikuhara, Mater. Trans. 43 (2002) 1517.
[30] M. Yoshimoto, T. Maeda, T. Ohnishi, H. Koinuma, O. Ishiyama, M. Shinohara, M. Kubo, R. Miura, A. Miyamoto, Appl. Phys. Lett. 67 (1995) 2615.